10-2013

Experimental investigation of the stent–artery interaction

Shijia Zhao
University of Nebraska-Lincoln

Linxia Gu
University of Nebraska-Lincoln, gul@fit.edu

Stacey R. Froemming
Children's Hospital and Medical Center, Omaha, NE

Published in *Journal of Medical Engineering & Technology* 37:7 (October 2013), pp. 463-469; doi: 10.3109/03091902.2013.831491

Submitted February 26, 2013; revised July 29, 2013; accepted July 31, 2013.

Experimental investigation of the stent–artery interaction

Shijia Zhao,[1] Linxia Gu,[1,2] and Stacey R. Froemming [3]

1. Department of Mechanical and Materials Engineering, University of Nebraska-Lincoln, Lincoln, NE 68588-0656, USA,
2. Nebraska Center for Materials and Nanoscience, Lincoln, NE 68588-0656, USA, and
3. Hybrid Catheterization & Electrophysiology Laboratory, Children's Hospital & Medical Center, Omaha, NE 68114-4133, USA

Corresponding author — L. Gu, email lgu2@unl.edu

Abstract

It is well acknowledged that stent implantation causes abnormal stretch and strains on the arterial wall, which contribute to the formation and progression of restenosis. However, the experimental characterization of the strain field on the stented vessel is scant. In this work, the balloon-expandable stent implantation inside an artery analogue was captured through two high-speed CCD cameras. The surface strain maps on the stented tube were quantified with a 3-D digital image correlation technique. The strain history at one specific reference point illustrated three stenting phases, including balloon inflation, pressurization and deflation. The surface strain distributions along one axial path were obtained at various time points to demonstrate the stent–vessel interactions. The radial wall thickness reduction history was used to evaluate the pressure–diameter relationship for the balloon. Results indicated that the expansion process of the balloon was significantly altered by the external loadings from both the stent and artery analogue. In addition, the repeatability of the stenting experiments was demonstrated through two tests with a change of 5% in the stent-induced maximum first principal strain. Moreover, a computational model of the stenting procedure was developed to recapture the stenting experiments. Comparison between experiments and simulation showed a difference of 7.17% in the first principal strain averaged over the high strain area. This indicated the validation of the computational framework, which can be used to investigate the strain or stress field throughout the computational domain, a feature that is not affected by experimental techniques.

Keywords: Balloon-expandable stent, digital image correlation, finite element method, surface strain measurement

1. Introduction

Stenting, a minimally invasive procedure to open the blocked arteries and restore blood flow, has gained popularity among cardiologists [1]. However, nearly one-third of stented patients require further intervention within 6 months to treat the reclosure of the lumen, i.e. restenosis [2,3]. Considerable strains on the vessel wall imposed by the stent have been linked to proliferation of smooth muscle cells, leading to restenosis [4–7]. Our previous numerical work has demonstrated a positive correlation between stent induced arterial strain or stress parameters with the reported restenosis rates [8]. Timmins et al. [9] also related the circumferential stress on the inner surface of artery to the neointimal thickness through porcine models. However, the existing quantifications of the strain or stress field on the artery are mainly obtained through numerical modeling. The experimental characterization of the stent-induced arterial strains is lacking. Squire et al. [10] performed the *in-vitro* strain measurement for stented bovine artery using one CCD camera. The x- and y-displacements of 40 reference points on the artery were captured during stent expansion and the strains were calculated using triads of reference points. Patel et al. [11] also measured the two-dimensional vascular strain induced by *in-vitro* balloon angioplasty using the ultrasound speckle tracking method. Horny et al. [12] conducted a preliminary study on evaluating the *in-vitro* deformation of human coronary artery induced by stent expansion using the digital image correlation (DIC) method; however, the comparison between separate experiments or between experiment and computational model was not performed.

In this work, two PALMAZ Genesis Transhepatic Biliary stents (PG5910B, Cordis Corporation, Warren, NJ) were implanted inside an artery analogue. The resulted three-dimensional deformations on the artery were captured and evaluated by a surface strain measurement system using two high-speed CCD cameras. In addition, a computational model has been developed to recapture the *in-vitro* stenting procedure. The validated computational model could be used to gather additional information inside the arterial wall where experimental methods are not effective. Thorough understanding of the stent–artery interactions that govern the arterial response is essential to further improve the stent design and lead to new insights into the mechanism of restenosis.

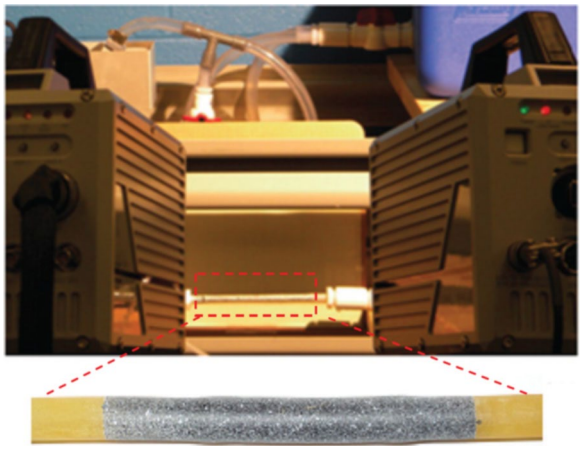

Figure 1. Experimental set-up with zoom view of the latex tube painted with stochastic pattern.

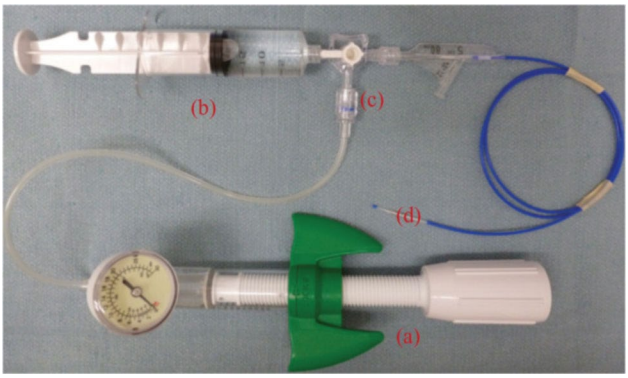

Figure 2. The stent delivery system, including inflation device (a), the syringe (b), the 3-way stopcock (c) and balloon catheter with crimped stent at its tip (d).

2. Materials and methods

2.1. Experimental set-up and procedure

An amber natural latex tube (Primeline Industries, Akron, OH) with an inner diameter of 6.32 mm, wall thickness of 1.55 mm and length of 170 mm was adopted to mimic a section of straight artery. Both ends of the latex tube were fixed onto two barbed hose connectors. A stochastic pattern of paint was sprayed on the outer surface of the tube to serve as reference points for digital image analysis. Two stereoscopically positioned high-speed cameras (up to 500 K frames s^{-1}) were used to take continuous pictures of all reference points (Figure 1). After all pictures were captured, the commercial 3-D image photogrammetry codes, ARAMIS (GOM mbH, Braunschweig, Germany), was used to analyze the deformation of the stented vessel. The analysis began by processing the first stereo pair of pictures, which describe the sample in its undeformed state. Each picture was divided into overlapping square or rectangular regions, i.e. facets. The start points were defined in the initial pair of pictures, with which the corresponding facets throughout them were found. Then the three-dimensional displacements over the deforming surface were calculated by matching corresponding facets in each successive picture across two cameras [13]. A detailed operational procedure of this measurement system can be found in our previous work [14].

The Z-MED II^{TM} balloon dilatation catheter (B. Braun Medical Inc., Bethlehem, PA) was used to deliver the stent to the targeted location (Figure 2). A PG5910B stent with a profile of 0.2 mm in strut thickness, 3.8 mm in inner diameter and 59 mm in length was originally crimped onto the balloon at the tip of the catheter. The catheter was connected to the balloon inflation device (B. Braun Medical Inc.) and the syringe via a 3-way stopcock to dilate the balloon as well as the stent on it.

During each test, the balloon catheter along with crimped stent was advanced to the centre of the latex tube. Then the inflation device infused water into the balloon to expand the stent. Following the manufacturer's specification, the balloon catheter pressure was slowly increased to 6 atm, held for 30 s and then decreased to 0 atm. At the end, the balloon was deflated and withdrawn along with the catheter from the vessel. The stent recoiled back and stayed in place to support the vessel. The deformation of vessel was captured at 0.5 frames s^{-1}. The surface strain map was obtained for every frame, which was also named as strain stage. The interval between two strain stages lasted 2 s. This stenting procedure was repeated twice in two latex tube sections.

2.2. Finite element simulation to reproduce the stenting experiment

The deployment of the PG5910B stent inside a latex tube was simulated to capture the *in-vitro* stenting test described above. Figure 3 shows the spatial relation between the crimped PG5910B stent and the latex tube before the expansion process. The crimped stent includes 16 repeating units along the axial direction and 11 units along the circumferential direction. The model was created using the plug-in 'WrapMesh' in Abaqus (Dassault Systèmes Simulia Corp., Providence, RI) to transform the planar configuration of the stent into the cylindrical shape. It was then meshed with 35 665 three-node triangular shell elements (S3R). The latex tube was modeled as a uniform hollow cylinder meshed with 18 000 reduced-integration eight-node brick elements (C3D8R). A mesh convergence study was carried out to guarantee a solution independent of the adopted mesh size.

Uniaxial tension tests were conducted on latex tube specimens to obtain its material properties in the axial and circumferential directions, as shown in Figure 4. It is clear that the latex tube material exhibits isotropic non-linear hyperelastic behavior. A reduced 3rd-order polynomial constitutive equation, as shown below, was used to fit the experimental data.

$$U = C_{10}(I_1 - 3)^1 + C_{20}(I_1 - 3)^2 + C_{30}(I_1 - 3)^3$$

where C_{i0} are material coefficients determined from the experimental data, while I_1 is the first invariant of the Cauchy-Green tensor in terms of principal stretch ratios λ_i as

$$I_1 = \lambda_1^2 + \lambda_2^2 + \lambda_3^2$$

The detailed description of fitting experimental data to the material model above can be found in our previous work [15]. The obtained material coefficients are C_{10} = 0.32588 MPa, C_{20} = −0.04572 MPa and C_{30} = 0.01174 MPa. The stent is made of 316L stainless steel with Young's modulus E = 190 GPa;

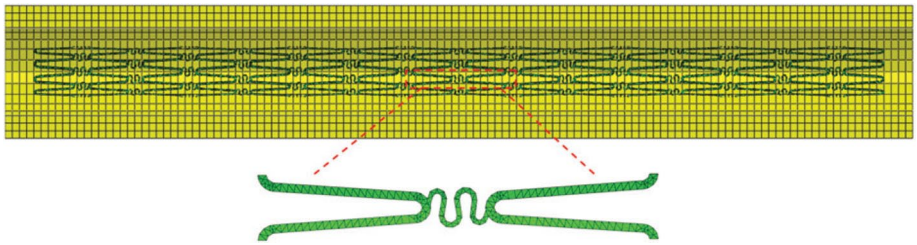

Figure 3. Three-dimensional model of the PG5910B biliary stent inside the latex tube.

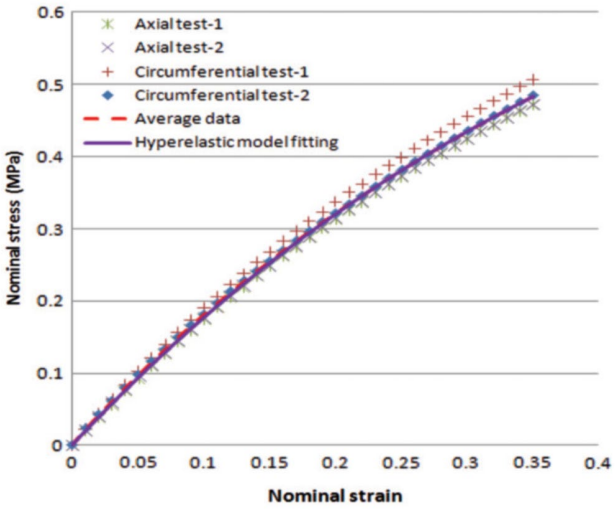

Figure 4. Uniaxial tension test results of the latex tube.

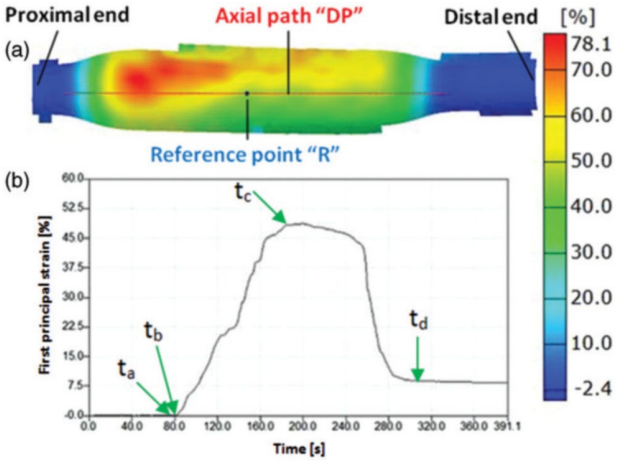

Figure 5. (a) The first principal strain distribution on the outer surface of latex tube at the time point of t_c, (b) the first principal strain history of the reference point 'R' during the stenting procedure.

Poisson ratio ν = 0.3; and Yield stress σ_Y = 207 MPa. The balloon expansion was driven by applying uniform radial displacement onto the inner surface of the balloon until the outer diameter of the latex tube reached the measured diameter of the stented latex tube. Both ends of the latex tube were fixed to capture the experimental conditions. Both ends of the stent were constrained with the rotational DOFs around radial and circumferential directions. The frictionless tangential contact behavior was used for all surface interactions, which are enforced based on the penalty method [16,17]. A typical simulation required ~14 h running in-parallel with all eight processors on a Dell T3500 workstation.

3. Results and discussions

3.1. Surface strain measurement on the outer surface of the stented artery analogue

During the *in-vitro* tests, the balloon pressure was increased up to 6 atm (expansion), held for 30 s (pressurization) and then decreased to 0 atm (recoil). This led to three distinct stages of arterial strain history, including its expansion, pressurization and recoil process, as shown in Figure 5. Figure 5(b) was created by tracking a single reference point, labeled as 'R' in Figure 5(a), over the duration of a single test. The first principal strain was then plotted over time. During the expansion phase, the arterial strain gradually increased to the peak value. The strain relaxed a little during the pressurization period. With the quicker release of balloon pressure, the artery recoiled back at a faster pace than that of the expansion phase. At the end, the equilibrium between the stretched latex tube and the scaffolding stent was gradually established after the withdrawal of the balloon catheter from the latex tube. In addition to the strain history of one single point, the strain components, including first principal strain, axial and circumferential strain, along the axial path 'DP', as shown in Figure 5(a), were used to demonstrate the stent–artery interactions at four specific timepoints, referred to as t_a to t_d.

Time point 't_a' represents the end-point of the initial flat region of the first principal strain history, as indicated in Figure 5. It was recorded after 76.6 s when the inflation pressure was ~2.39 atm. At this time, the stent was not expanded enough to come into contact with the inner wall of the latex tube. Both the circumferential and axial strain components were minimal at this stage, as shown in Figure 6(a). This might be due to the environmental noise [10], which was validated by undertaking a zero-strain test and the magnitude of first principal strain reached 0.155%. At the 78.6 s point (t_b) when the inflation pressure was ~2.45 atm, the distal end of the stent began to come into contact with the inner surface of the latex tube and an abrupt increase in the strain magnitude in the distal region of the stent was observed, as shown in Figure 6(b). At this point, the value of maximum first principal strain was 0.73%, which is 5.6-times greater than the maximum strain measured 2 s earlier. At the 183 s point (t_c) the peak first principal strain of 66% was observed, as shown in Figure 6(c), when the balloon pressure was increased to 6 atm. The length of the artery analogue with higher strain value is 40.56 mm, which is close to the balloon length of 40 mm. This indicates that the artery is fully in contact with both the stent and balloon. It is worth noting that the two peak first principal strains of 66% and 47% were located at

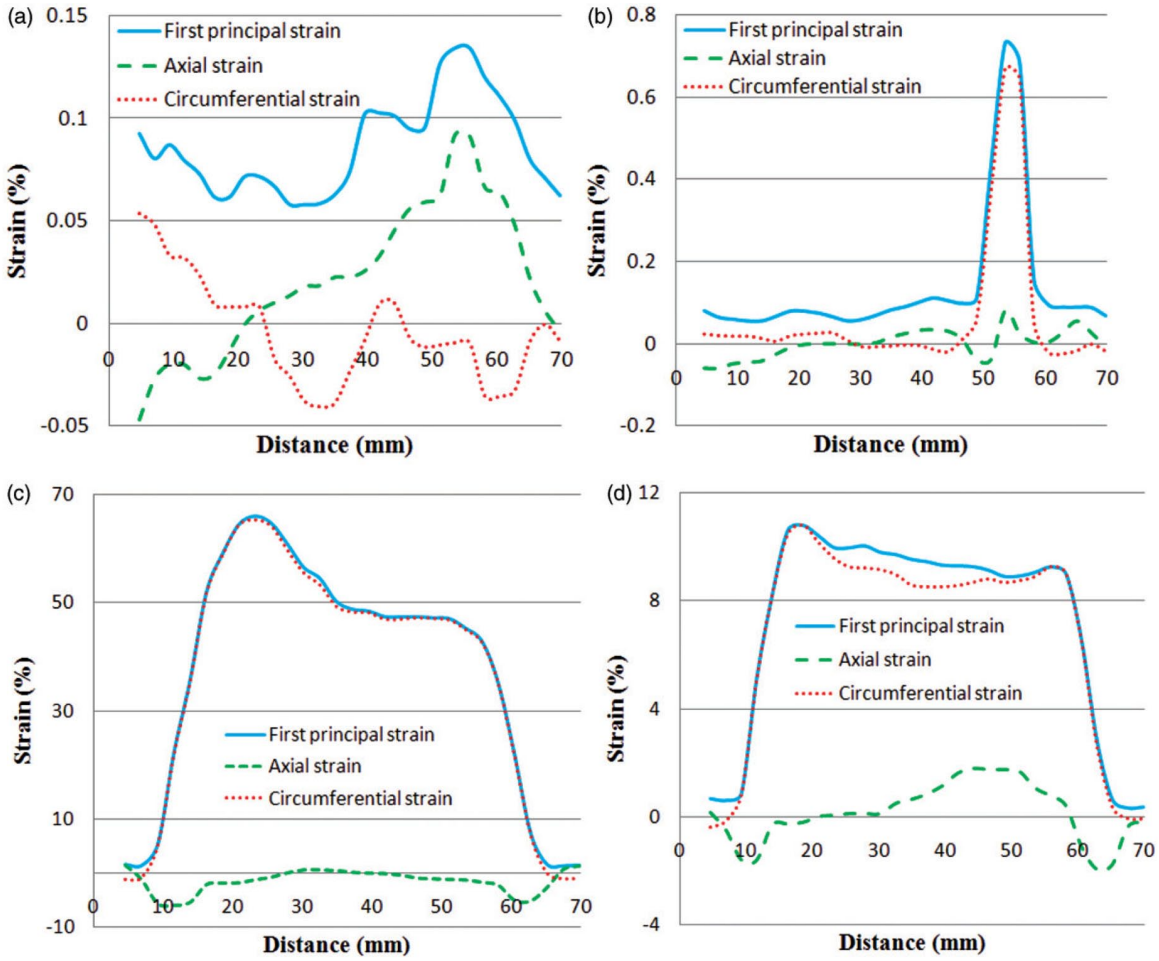

Figure 6. The strain distribution along the axial path DP at time points (a) t_a = 76.6 s, (b) t_b = 78.6 s, (c) t_c = 183 s and (d) t_d = 298 s.

the two ends of the axial path. This might be explained by the non-uniform expansion of the balloon catheter. It is also interesting to observe that the first principal strain and circumferential strain have almost the same magnitude, indicating the circumferential strain is the dominant mode after the complete contact between stent and artery. After the balloon was deflated and withdrawn from the artery, the equilibrium between plastic deformation of stent and spring back load of the latex tube was achieved after 298 s (t_d). The distribution of strain components along the path 'DP' is shown in Figure 6(d), where the first principal strain magnitude decreased from a value of 66% to a value of 10.8%, which is the strain obtained after 183 s. This excessive recoil is due to the stiffer latex material compared to the native artery.

3.2. Radial deformation measurement

The radial deformation in terms of thickness reduction, which was calculated from first and second principal strains, was also obtained. The temporal variation of the thickness reduction for the reference point 'R' is plotted in Figure 7(a), while the spatial variation of the thickness reduction along the axial path 'DP' was plotted at time point t_c, as shown in Figure 7(b). It is clear that both the temporal and spatial distribution of the thickness reduction exhibit similar trends as the first principal strain. This could be explained by the consistent volume theory. The reduction in the wall thickness in response to the stent-induced surface deformation is to maintain a constant volume for the artery analogue.

3.3. Pressure–diameter relationship of the balloon

The diameter of the expanded artery analogue was also obtained through the cylinder fitting function in the ARAMIS system. The history of the outer diameter of the latex tube at the reference point 'R' is depicted in Figure 8. It exhibited a similar trend as its first principal strain history. This diameter history was used to estimate the diameter of balloon by subtracting both the thickness reduction in Figure 7(a) and stent thickness of 0.2 mm. Then the pressure-diameter curve for the balloon could be obtained and compared to the nominal expansion data provided by the manufacturer, as depicted in Figure 9. It is clear that the experimentally obtained balloon expansion history has a distinctly different path than the one provided by the manufacturer, although both of these paths reached plateau at the final stage. The difference could be due to the external loading conditions since the nominal data is usually tested in the air, which is not the case in the stenting operations. This indicated that the expansion behavior of the balloon was dramatically altered by the external loading environments, such as the stent and latex tube in our case. Results also implied that careful consideration of the lesion loadings is necessary to enhance the stenting outcomes.

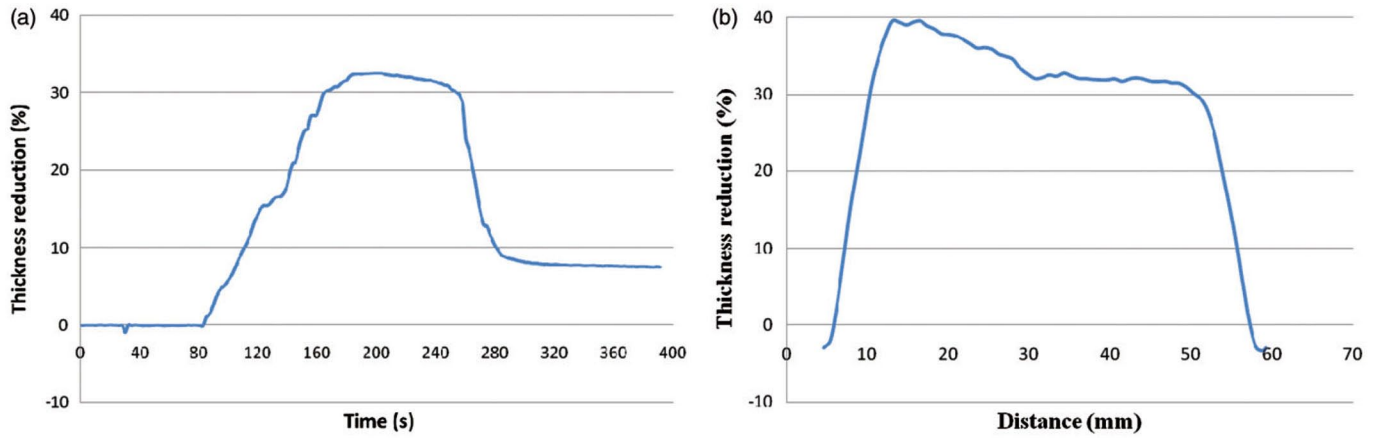

Figure 7. (a) The temporal variation of thickness reduction for the reference point 'R'; (b) the thickness reduction along the axial path 'DP' captured at 183 s (t_c).

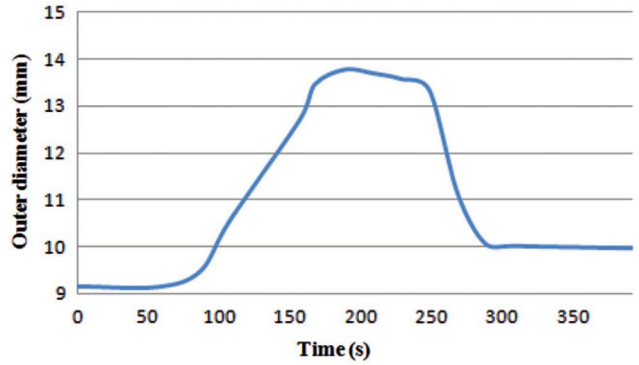

Figure 8. The outer diameter history of the stented latex tube.

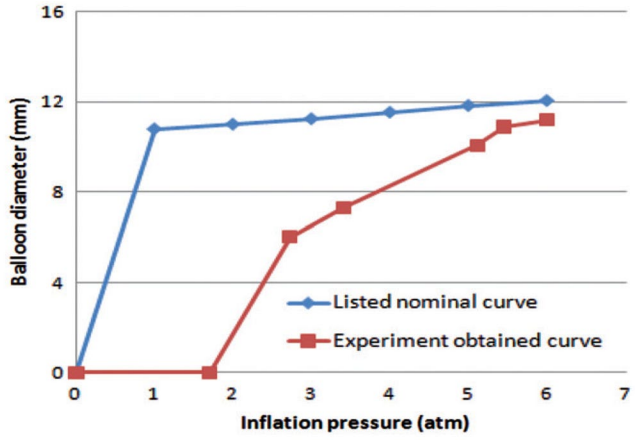

Figure 9. The pressure–diameter relationship of the balloon.

3.4. Finite element model validation

The surface strain distributions from two experimental stenting tests demonstrated repeatable distributions, as shown in Figure 10, where the first principal strain distribution along the axial path 'DP' of the stented latex surface is plotted at time after 298 s. The maximum first principal strain in both tests was measured as 9.45% and 9.95%. The relative change

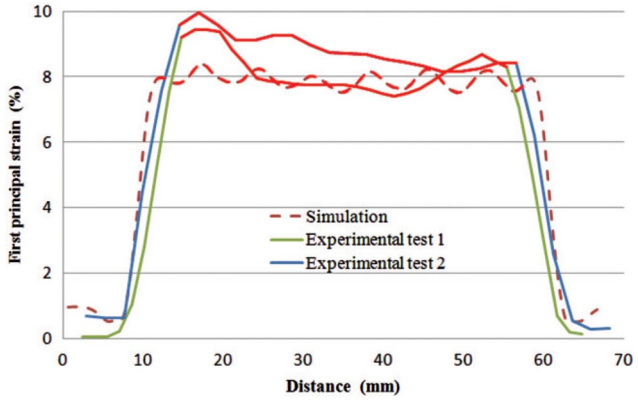

Figure 10. Comparisons of the stent-induced first principal strain profiles.

between these maximum strain values is ~5%. The average strain on the portion of the axial path where higher strain occurred due to stent expansion, as highlighted in red in Figure 10, was 8.18% and 8.83% for the two tests, respectively. The relative change between these two average strain values is ~7%. The length of the stented area, measured as the length of the aforementioned highlighted higher strain portion of the axial path, was 40.56 mm and 41.94 mm, respectively. The difference could be due to the mismatch of axial path between the two tests. The opaqueness of the painted latex tube prevents identification of the same surface path, i.e. the exact area of contact with the expanded stent. The small difference of strain value between these tests suggests good repeatability of the experiment.

Further quantitative measures of the relationship between stent deign and arterial mechanics can be enhanced with use of an FE model, which was developed to reproduce the stenting experiments. The obtained results were compared to experimental measurements and a good agreement was observed, as shown in Figure 10. It is clear that the simulated strain profile along the axial path was symmetric and relatively uniform. The maximum first principal strain found in the simulation was reported as 8.39%, which is 1.31% less than the averaged peak first principal strain value from the experiment of 9.70%. The average value of the aforementioned averaged higher strain in two experiments was 8.51%; while it was calculated as 7.90% based on the red portion

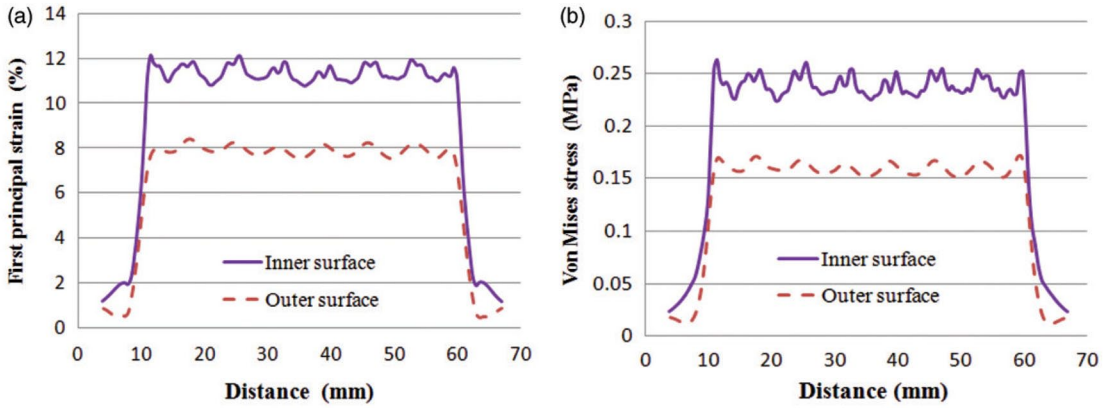

Figure 11. Comparisons of (a) first principal strain and (b) Von Mises stress between the inner surface and outer surface of the stented latex tube.

of the first principal strain–distance curve from the simulation result. The relative error between the averaged strain value from the two experiments (8.51%) and the strain value from simulation (7.90%) is calculated as 7.17%, which is acceptable for most engineering applications. This validated our computational framework for further stenting investigations. Once the computational model was validated, it provides the virtual platform for testing a wide variety of conditions including clinical settings.

3.5. Strain and stress parameter within the arterial wall

The strain or stress field on the internal surface of the artery has been studied previously due to the direct contact surface between the stent and artery [8,10]. However, it is not easily measured by optical measurements on the exterior surface. The computational model can be used to investigate the strain or stress field anywhere within the computational domain [8,18,19], a feature that is not affected by experimental techniques.

The comparison of the first principal strain and Von Mises stress between the inner and outer surface of the stented latex tube are plotted in Figure 11(a) and (b), respectively. It is clear that the inner surface exhibited a relative larger magnitude and variation of both wall strain and stress than the outer surface. This indicates that the strut structure has a more significant influence on the strain or stress field on the inner surface. This was consistent with clinical studies [20], which demonstrated that the stent expansion-induced large strains on intimal surface of stenotic vessel might be the determinant of in-stent restenosis. The validated computational model in this work could provide more insight about the stent–artery interaction, which will in turn facilitate the development of new stent designs.

4. Conclusions

In this work an *in-vitro* stenting procedure in an artery analogue was captured by two high-speed CCD cameras. The variation of surface strain and changes in thickness in both temporal and spatial domain were quantified using a 3-D digital image correlation technique, which provides better understanding of the artery deformation during stent expansion. Two tests were conducted and the small relative change in measured strain indicates the repeatability of experiments. A computational model was developed to recapture the stenting experiment. The agreement between the experimental results and the computational results led to the validation of the computational framework, within this particular experimental context. The experiment-validated computational framework can then be used to estimate the stent–artery interactions under various conditions including clinical settings. To better mimic the physiological conditions, future stenting tests will be conducted inside a porcine artery immersed in a 37 °C saline bath with blood analogue circulated inside and the anisotropic material model of the artery wall will be adopted. The viscoelasticity of the artery will also be considered when defining its mechanical properties. The displacement boundary condition was used to expand the balloon in this work, while the pressure-driven folded balloon model might provide more details about balloon–stent interaction and will be incorporated in our future works. The computational results could be further used to correlate with the cellular response and tissue re-modeling following the stent implantation [21].

Acknowledgments — The support of the National Science Foundation under grant No. 0926880 is gratefully acknowledged. The authors thank Mr. Jonathan Hein for operating the ARAMIS system during experiments.

References

1. Early, M., Lally, C., Prendergast, P.J., and Kelly, D.J., 2009, Stresses in peripheral arteries following stent placement: A finite element analysis. Computer Methods in Biomechanics & Biomedical Engineering, 12, 25–33
2. Sumpio, B.E., Banes, A.J., Levin, L.G., and Johnson, G., Jr., 1987, Mechanical stress stimulates aortic endothelial cells to proliferate. Journal of Vascular Surgery, 6, 252–256
3. Schillinger, M., Sabeti, S., Loewe, C., Dick, P., Amighi, J., Mlekusch, W., Schlager, O., Cejna, M., Lammer, J., and Minar, E., 2006, Balloon angioplasty versus implantation of nitinol

stents in the superficial femoral artery. New England Journal of Medicine, 354, 1879–1888

4. Steinman, D.A., Vorp, D.A., and Ethier, C.R., 2003, Computational modeling of arterial biomechanics: Insights into pathogenesis and treatment of vascular disease. Journal of Vascular Surgery, 37, 1118–1128
5. Schwartz, E.A., Bizios, R., Medow, M.S., and Gerritsen, M.E., 1999, Exposure of human vascular endothelial cells to sustained hydrostatic pressure stimulates proliferation. Involvement of the alphaV integrins. Circulation Research, 84, 315–322
6. Becker, G.J., 1991, Intravascular stents. General principles and status of lower-extremity arterial applications. Circulation, 83 (Suppl 2), I122–136
7. Oesterle, S.N., Whitbourn, R., Fitzgerald, P.J., Yeung, A.C., Stertzer, S.H., Dake, M.D., Yock, P.G., and Virmani, R., 1998, The stent decade: 1987 to 1997. Stanford Stent Summit faculty. American Heart Journal, 136, 578–599
8. Gu, L.X., Zhao, S.J., Muttyam, A.K., and Hammel, J.M., 2010, The relation between the arterial stress and restenosis rate after coronary stenting. Journal of Medical Devices, 4, 031005
9. Timmins, L.H., Miller, M.W., Clubb, F.J., and Moore, J.E., 2011, Increased artery wall stress post-stenting leads to greater intimal thickening. Laboratory Investigation, 91, 955–967
10. Squire, J.C., Rogers, C., and Edelman, E.R., 1999, Measuring arterial strain induced by endovascular stents. Medicine & Biological Engineering in Computing, 37, 692–698
11. Patel, P., Biswas, R., Park, D., Cichonski, T.J., Richards, M.S., Rubin, J.M., Phan, S., Hamilton, J., and Weitzel, W.F., 2010, Characterization of vascular strain during *in-vitro* angioplasty with high-resolution ultrasound speckle tracking. Theoretical Biology & Medical Modelling, 7, 36
12. Horny, L., Chlup, H., Zitny, R., Vonavkova, T., Vesely, J., and Lanzer, P., 2012, *Ex vivo* coronary stent implantation evaluated with digital image correlation. Experimental Mechanics, 52, 1555–1558
13. Zwierzak, I., Fenner, J.W., and Narracott, A.J., 2011, Strain measurement in an elastic material under large deformation using optical reconstruction methods. In: Vlad, S., and Ciupa, R. V., editors. IFMBE Proceedings (Berlin: Springer), 36, pp. 120–123
14. Steinert, B.D., Zhao, S.J., and Gu, L.X., 2012, Mapping mechanical strain distributions on the surface of stented vessel. Journal of Visualized Experiments, 10, 300–305
15. Zhao, S.J., Gu, L.X., Hammel, J.M. and Lang, H.L., 2010, Mechanical behavior of porcine pulmonary artery (Vancouver, British Columbia, Canada: ASME International Mechanical Engineering Congress and Exposition)
16. Oden, J.T., 1981, Exterior penalty methods for contact problems in elasticity. In: Wunderlich, K.J.B.W., and Stein, E., editors. Nonlinear Finite Element Analysis in Structural Mechanics (Berlin: Springer), pp. 655–665
17. Laursen, T.A., 2002, Computational contact and impact mechanics: Fundamentals of modeling interfacial phenomena in nonlinear finite element analysis. In: Laursen, T. A., editor. Engineering Online Library (Berlin, New York: Springer), pp. 89–91
18. Lally, C., Dolan, F., and Prendergast, P.J., 2005, Cardiovascular stent design and vessel stresses: A finite element analysis. Journal of Biomechanics, 38, 1574–1581
19. Zahedmanesh, H., John Kelly, D., and Lally, C., 2010, Simulation of a balloon expandable stent in a realistic coronary artery -- Determination of the optimum modelling strategy. Journal of Biomechanics, 43, 2126–2132
20. Geary, R.L., Nikkari, S.T., Wagner, W.D., Williams, J.K., Adams, M.R., and Dean, R.H., 1998, Wound healing: A paradigm for lumen narrowing after arterial reconstruction. Journal of Vascular Surgery, 27, 96–108
21. Yazdani, S.K., and Berry, J.L., 2009, Development of an in vitro system to assess stent-induced smooth muscle cell proliferation: A feasibility study. Journal of Vascular and Interventional Radiology, 20, 101–106